Communication

A Novel Method for Beampattern Synthesis With Auto-Determined Minimum Mainlobe Width

Tianyuan Gu, Xuejing Zhang, Kejiang Wu, Kangning Li, Wei Cui, and Qing Shen

***Abstract*—This communication presents a beampattern synthesis method with auto-determined minimum mainlobe width named reweighted domino norm and spectral factorization (RD-SF). To improve the computational efficiency, a RD-l_1 norm is constructed to solve monotonic sparse optimization problems without monotonicity constraints. In addition, a spectral factorization (SF)-based method without rank 1 constraint is also used to solve the nonconvex constraints of shaped beampattern. On the basis of RD-SF method, we utilize a two-step spatial response variation (SRV) scheme to synthesize frequency-invariant (FI) broadband beampattern. It is regarded as the broadband version of the RD-SF method, named RD-SF-broadband (RD-SF-B). This scheme avoids redundant SRV constraints while maintaining an undistorted mainlobe. Moreover, the approximation error does not need to be set. Simulation results are shown to verify the effectiveness of our proposed algorithm.**

***Index Terms*—Auto-determined minimum mainlobe width, frequency-invariant (FI), reweighted domino norm, shaped beampattern, spectral factorization (SF), two-step spatial response variation (SRV).**

I. Introduction

Antenna array pattern synthesis plays an important role in various fields, such as radar, navigation, wireless communication, and so on [1]. For instance, the classical Chebyshev algorithm is proposed in [2] and the connection between array element and beampattern was revealed in [3]. These methods can give the closed-form solutions but are limited by some specific array geometries. With the development of optimization theory, a stream of methods based on global-optimization emerged [4], [5], [6]. The common disadvantage of these methods is that they are time-consuming. Since the introduction of convex optimization [7], numerous algorithms leveraging convex optimization are developed. Assisted by convex programming, beampattern level was constrained in [8].

To ensure the mainlobe direction in high-speed motion scenarios, comparing to focused beampattern, shaped beampattern makes a huge difference in radar and wireless communication because of the improvement it brings to system capacity and convergence. With the application of convex optimization theory in the synthesis of shaped beampattern, the mainlobe ripple level and sidelobe level are usually needed to be constrained. However, the lower bound constraint of the mainlobe ripple level is nonconvex. To transform the lower bound constraint into a convex one, the semidefinite relaxation (SDR) [9] is utilized in [10], where the response of the beampattern is relaxed by constructing a symmetric positive semidefinite matrix of rank one. Moreover, shaped beampattern synthesis can be constructed as a convex optimization model through linear programming method [11] and sequential convex optimization [12].

With the increasing need for signal bandwidth in radar and communication systems, the research on broadband array [13], especially the study of frequency-invariant (FI) beampattern which may avoid mainlobe distortion when the array receives broadband signals, has attracted widespread attention [14], [15]. There have been some methods for synthesizing FI beampattern [16], [17]. These methods have limitations in controlling sidelobe levels and dependence on the reference pattern. With the help of convex optimization, the spatial response variation (SRV) method was proposed in [18].

Mainlobe width is a necessary parameter in beampattern design. It has a trade-off relationship with mainlobe and sidelobe level [19]. The beampattern design problem can also be regarded as a magnitude filter design problem [20]. When designing beampattern synthesis, it is usually necessary to set the angular region of mainlobe and sidelobe to apply different constraints. The width of these angular regions are usually set relied on experience. Moreover, for diverse shaped beampatterns, the width of mainlobe is even more difficult to calculate. Improper setting of mainlobe width can result in unsolvable or unsatisfactory beampattern performance. Therefore, based on relaxation optimization, there have already emerged some beampattern synthesis methods with auto-determined minimum mainlobe width [21], [22], [23], [24], [25], [26], [27] recently. Building upon existing relaxation-variable techniques and inspired by finite impulse response filter design principles in [28], this communication proposes the reweighted domino-norm and spectral factorization (RD-SF) method for beampattern synthesis with minimum auto-determined mainlobe width. The spectral factorization (SF) approach transforms the nonconvex lower bound constraint on mainlobe ripple level into a convex formulation, enabling reference-free shaped beampattern synthesis.

Without the rank-one constraint, the SF method can achieve higher computational efficiency than comparable algorithms (e.g., SDR). Moreover, Huan et al. [25] proposed the domino-l_0 norm to avoid monotonicity constraints when synthesizing a 3-D beampattern. By transforming the domino-l_0 norm to a 2-D version, we construct the RD-l_1 norm to achieve sparse optimization. In the broadband FI case, methods based on SRV constraints [18], [23], [27] rely on an empirically determined angular region that encompasses the mainlobes to approximate at different frequencies.

Typically, the angular region corresponds to the initial relaxation region. However, overly broad relaxation regions necessitate excessive SRV constraints. Critically, while the two-step method [26] precisely defines mainlobe boundaries, it omits mainlobe level constraints which can ensures mainlobe undistorted. To leverage the complementary strengths of both approaches, we implement a two-step SRV scheme: first, the RD-SF method determines the minimum achievable mainlobe width. Subsequently, SRV constraints are applied to mainlobe regions across other frequencies, leading to the RD-SF-Broadband (RD-SF-B) method. This hybrid approach enables stable and efficient synthesis of FI broadband beampatterns. Notably, the second-step objective function is the approximation error of cross-frequency mainlobe level which enable it to generate nonempirically. Highlights are summarized as follows.

Received 7 May 2025; revised 24 July 2025; accepted 8 August 2025. Date of publication 21 August 2025; date of current version 18 December 2025. This work was supported in part by the National Natural Science Foundation of China under Grant 62401055, Grant 62271052, and Grant 62531016; in part by Sichuan Science and Technology Program under Grant 2024NSFSC1433; and in part by the Peng Cheng Shang Xue Education Fund under Grant XY2021602. *(Corresponding author: Kejiang Wu.)*

Tianyuan Gu, Kejiang Wu, Kangning Li, Wei Cui, and Qing Shen are with the School of Information and Electronics, Beijing Institute of Technology, Beijing 100081, China (e-mail: tygu0607@163.com; wukejiang88@163.com; qing-shen@outlook.com).

Xuejing Zhang is with the School of Information and Communication Engineering, University of Electronic Science and Technology of China, Chengdu 611731, China (e-mail: xjzhang7@163.com).

Digital Object Identifier 10.1109/TAP.2025.3599317

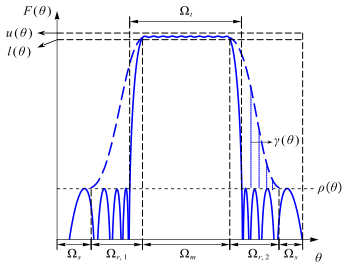

Fig. 1. Illustration for the shaped beam.

1) *Narrowband beampattern synthesis (RD-SF):*
   a) Using SF method to transform nonconvex lower bound constraint avoids rank one constraint.
   b) RD-l_1 norm enhances the sparsity of l_0 norm without complex monotonicity constraints.
2) *Broadband FI beampattern synthesis (RD-SF-B):*
   a) Two-step SRV scheme prevents mainlobe distortion and redundant SRV constraints simultaneously.
   b) Minimum mainlobe approximation error can be obtained automatically.

II. Preliminaries

In this section, we will show the basic optimization model of beampattern synthesis. For a uniform linear array (ULA) with N elements, the steering vector is given as

$$\mathbf{a}(\theta) = \left[1, e^{j\Phi}, \ldots, e^{j(N-1)\Phi}\right]^{\mathrm{T}} \tag{1}$$

where $\Phi = 2\pi d\sin(\theta)/\lambda$, d is the element spacing and λ is the signal wavelength. The beampattern of this antenna array can be expressed as

$$F(\theta) = \mathbf{w}^{\mathrm{H}}\mathbf{a}(\theta) \tag{2}$$

where

$$\mathbf{w} = [w_0, w_1, \ldots, w_{N-1}]^{\mathrm{T}} \tag{3}$$

is weight vector. Then, the shaped beampattern synthesis is given

$$\text{find } \mathbf{w} \tag{4a}$$
$$\text{s.t. } l(\theta) \le |\mathbf{w}^{\mathrm{H}}\mathbf{a}(\theta)|^2 \le u(\theta), \quad \theta \in \Omega_m \tag{4b}$$
$$|\mathbf{w}^{\mathrm{H}}\mathbf{a}(\theta)|^2 \le \rho(\theta), \quad \theta \in \Omega_s. \tag{4c}$$

As proven in [29], $|\mathbf{w}^{\mathrm{H}}\mathbf{a}(\theta)|^2 \ge l(\theta)$ in (4b) is nonconvex.

To highlight the advantages of SF algorithm, we take the shaped beampattern as the example. If a focused beampattern needs to be synthesized, just replace constraint (4b) with

$$\mathbf{w}^{\mathrm{H}}\mathbf{a}(\theta) = 1. \tag{5}$$

As shown in Fig. 1, Ω_m stands for the angular region of the shaped mainlobe, and Ω_s denotes the angular region of the sidelobe. $\rho(\theta)$ is the upper bound of the region Ω_s, while $u(\theta)$ and $l(\theta)$ are the upper and lower bound of the Ω_m region, respectively. However, there are two transition regions $\Omega_{r,1}$, $\Omega_{r,2}$ whose width are usually set by experience. It is our target to synthesize beampattern with Ω_t automatically, ignoring the effect of $\Omega_{r,1}$ and $\Omega_{r,2}$.

III. Proposed Algorithm

In this section, we will provide a detailed introduction to our proposed RD-SF and RD-SF-B method, including the beampattern synthesis method based on SF, the minimum mainlobe synthesis method based on relaxation optimization, and the FI broadband beampattern synthesis method based on two-step SRV strategy. As the focused beampattern represents a special case of the shaped beampattern, we focus on the shaped beampattern optimization model in the subsequent analysis.

A. Beampattern Constraints via SF

The constraint in (4b) is inherently nonconvex. In order to solve this problem, a new vector with length of $2N-1$ is introduced

$$\mathbf{b}(\theta) = \left[e^{-j(N-1)\Phi}, \ldots, e^{-j\Phi}, 1, e^{j\Phi}, \ldots, e^{j(N-1)\Phi}\right]^{\mathrm{T}}. \tag{6}$$

Then, the following relationship is obtained, that is,

$$|F(\theta)|^2 = \left[\mathbf{w}^{\mathrm{H}}\mathbf{a}(\theta)\right]\left[\mathbf{w}^{\mathrm{H}}\mathbf{a}(\theta)\right]^* = \mathbf{r}_w^{\mathrm{T}}\mathbf{b}(\theta) \tag{7}$$

where

$$\mathbf{r}_w = [r_w(-N+1), \ldots, r_w(0), \ldots, r_w(N-1)]^{\mathrm{T}} \tag{8}$$

with

$$r_w(n) = \sum_{i=0}^{N-|n|-1} w_i w_{i+n}^*, \quad n = -N+1, \ldots, 0, \ldots, N-1. \tag{9}$$

Here, $r_w(n)$ denotes the autocorrelation function of w_n and holds the following properties:

$$r_w(-n) = r_w^*(n) \tag{10}$$
$$r_w(0) \ge 0. \tag{11}$$

So, the $\mathbf{r}_w^{\mathrm{T}}\mathbf{b}(\theta)$ in (7) can be further expanded into a polynomial

$$\mathbf{r}_w^{\mathrm{T}}\mathbf{b}(\theta) = T\left(e^{j\Phi}\right) = \sum_{n=-N+1}^{N-1} r_w(n) e^{jn\Phi}. \tag{12}$$

Then, construct a new polynomial $P(e^{j\Phi})$ by multiplying $e^{j(N-1)\Phi}$ and $T(e^{j\Phi})$, given by

$$P\left(e^{j\Phi}\right) = e^{j(N-1)\Phi}T\left(e^{j\Phi}\right) = \sum_{n=-N+1}^{N-1} r_w(n) e^{j(N-1+n)\Phi}. \tag{13}$$

Denote σ as a zero of $P(e^{j\Phi})$, that is, $P(\sigma) = 0$. Property (10) directly implies $T(e^{-j\Phi}) = T^*(e^{j\Phi})$. Then, we have

$$P\left(\sigma^{-1}\right) = \sigma^{-(N-1)}T\left(\sigma^{-1}\right) = \sigma^{-(N-1)}T^*(\sigma) = 0. \tag{14}$$

In other words, σ^{-1} is also a zero point of $P(e^{j\Phi})$. Denote $\sigma_1, \sigma_2, \ldots, \sigma_{N-1}$ as the $N-1$ roots of $P(e^{j\Phi})$ which are inside the unit circle. The roots exhibit conjugate symmetry: $1/\sigma_1^*, 1/\sigma_2^*, \ldots, 1/\sigma_{N-1}^*$. Then we can factorize $P(e^{j\Phi})$ into

$$P\left(e^{j\Phi}\right) = \mu\prod_{i=1}^{N-1}\left(e^{j\Phi} - \sigma_i\right)\left(\sigma_i^* e^{j\Phi} - 1\right) \tag{15}$$

where μ is a positive constant, and $T(e^{j\Phi})$ can be factorized into

$$T\left(e^{j\Phi}\right) = e^{-j(N-1)\Phi}P\left(e^{j\Phi}\right) = \mu\prod_{i=1}^{N-1}\left(1 - \sigma_i e^{-j\Phi}\right)\left(\sigma_i^* e^{j\Phi} - 1\right). \tag{16}$$

Finally, we define the spectral factor as

$$S\left(e^{j\Phi}\right) = \sqrt{\mu}\prod_{n=1}^{N-1}\left(1 - \sigma_n e^{-j\Phi}\right). \tag{17}$$

However, we have a relationship as following:

$$\mathbf{r}_w^{\mathrm{T}}\mathbf{b}(\theta) = T\left(e^{j\Phi}\right) = S\left(e^{j\Phi}\right)S\left(e^{-j\Phi}\right) \tag{18}$$

where $S(e^{j\Phi}) = w_0 + w_1 e^{j\Phi} + w_2 e^{j2\Phi} + \cdots + w_{N-1}e^{j(N-1)\Phi}$, stands for the beampattern function.

Hence, we are able to construct the weight vector $\mathbf{w}$ which consists of the coefficients of $S(e^{j\theta})$. More detailed principles of SF can be found in [26]. Therefore, with the properties in (10) and (11), the constraints (4b) and (4c) can be rewritten

$$l(\theta) \le \mathbf{r}_w^{\mathrm{T}}\mathbf{b}(\theta) \le u(\theta), \quad \theta \in \Omega_m \tag{19a}$$
$$\mathbf{r}_w^{\mathrm{T}}\mathbf{b}(\theta) \le \rho(\theta), \quad \theta \in \Omega_s. \tag{19b}$$

It is worth mentioning that the constraint (19a) is a convex constraint applied in FIR filter design [28] which can also be used to synthesize shaped beampatterns. To recover the weight vector $\mathbf{w}$, we can first construct the polynomial in (12) with the obtained $\mathbf{r}_w$. Then, find the roots of the polynomial $T(e^{j\Phi})$ within the unit circle. Finally, construct the polynomial $S(e^{j\Phi})$ in (17) and take the coefficients of each term as the weight vector $\mathbf{w}$.

B. Sparse Optimization for Relaxation Variables

It is known that many existing algorithms rely on experience to set the width of the transition region. The difference of our proposed algorithm is that we minimize the width of the initial relaxation region by iteratively optimizing the relaxation variables in it. After iterations, the relaxation region we get is the narrowest transition region.

To begin with, we introduce relaxation variables onto $\Omega_{r,1}, \Omega_{r,2}$ shown in Fig. 1. Different from the strict constraints in (4c), the constraint in the relaxation region is written as

$$\mathbf{r}_w^{\mathrm{T}}\mathbf{b}(\theta) \le \rho(\theta) + \gamma(\theta), \quad \theta \in \Omega_{r,1} \cup \Omega_{r,2} \tag{20}$$

where $\gamma(\theta) \ge 0$.

To generate a smooth transition band, the monotonicity of $\gamma(\theta)$ also needs to be considered. According to the shape of a beampattern (e.g., Fig. 1), $\gamma(\theta)$ should be monotonically nondecreasing in $\Omega_{r,1}$ and monotonically nonincreasing in $\Omega_{r,2}$.

First, we might as well discretize the angle in $\Omega_{r,1}$ and $\Omega_{r,2}$

$$\begin{cases} \Omega_{r,1} \Rightarrow \{\theta_{1,1}, \theta_{1,2}, \ldots, \theta_{1,R}\} \\ \Omega_{r,2} \Rightarrow \{\theta_{2,R}, \theta_{2,R-1}, \ldots, \theta_{2,1}\} \end{cases} \tag{21}$$

where R_1 and R_2 denote the endpoint of $\Omega_{r,1}$ and $\Omega_{r,2}$ separately.

Denote the relaxation variable as

$$\Gamma = \left[\gamma(\theta_{1,1}), \ldots, \gamma(\theta_{1,R}), \gamma(\theta_{2,R}), \ldots, \gamma(\theta_{2,1})\right]^{\mathrm{T}}. \tag{22}$$

Satisfying monotonicity implies that as the number of zero-value relaxation variables increases, the dashed line (initial relaxation region) in Fig. 1 approaches the solid line (desired transition band). Hence, we are able to transform the transition bandwidth minimization problem into a sparse optimization problem of Γ

$$\min_{\Gamma} \ \|\Gamma\|_0 \tag{23}$$

where $\|\cdot\|_0$ is the l_0 norm operation.

In order to avoid numerous monotonic constraints, inspiring by the domino norm proposed in [25], we modify a 2-D version. To satisfy the knocking down order of domino norm, we should arrange the elements of relaxation variable from outside to inside in pairs like

$$\Gamma = \left[\underbrace{\{\gamma(\theta_{1,1}), \gamma(\theta_{2,1})\}}_{\gamma_1}, \ldots, \underbrace{\{\gamma(\theta_{1,R}), \gamma(\theta_{2,R})\}}_{\gamma_R}\right]^{\mathrm{T}}. \tag{24}$$

Then, calculate the maximum value of each pair of elements in Γ

$$g(\gamma_r) = \max_{r=1,2,\ldots,R} \{\gamma(\theta_{1,r}), \gamma(\theta_{2,r})\}. \tag{25}$$

Subsequently, construct the so-called domino vector $\mathbf{G}(\Gamma)$

$$\mathbf{G}(\Gamma) = \begin{bmatrix} g(\gamma_1) \\ \frac{1}{2}(g(\gamma_1) + g(\gamma_2)) \\ \vdots \\ \frac{1}{R}(g(\gamma_1) + g(\gamma_2) + \cdots + g(\gamma_R)) \end{bmatrix}. \tag{26}$$

Since the different optimization priorities corresponding to elements in $\mathbf{G}(\Gamma)$, the sparse optimization problems with monotonicity can be denoted as

$$\min_{\Gamma} \ \|\mathbf{G}(\Gamma)\|_0. \tag{27}$$

Algorithm 1 Proposed RD-SF Algorithm

1: **Input:** $u(\theta), l(\theta), \rho(\theta), N, \epsilon, \Omega_m$.
2: **Initialize:** $\Omega_s, \Omega_r, \gamma^{(0)} = [1, 1, \ldots, 1]^{\mathrm{T}}$.
3: Construct $g^{(i-1)}(\gamma_1), g^{(i-1)}(\gamma_2), \ldots, g^{(i-1)}(\gamma_R)$.
4: **while** no convergence **do**
5: $\mathbf{A}^{(i)} = [\alpha_1^{(i)}, \alpha_2^{(i)}, \ldots, \alpha_R^{(i)}]^{\mathrm{T}}$ with $\alpha_r^{(i)} = \left(|\frac{1}{r}(g^{(i-1)}(\gamma_1) + g^{(i-1)}(\gamma_2) + \cdots + g^{(i-1)}(\gamma_r))| + \epsilon\right)^{-1}$.
6: Solve problem (29) and obtain desired $\mathbf{r}_w$.
7: **end while**
8: Recover $\mathbf{w}$ through the SF method.
9: **Output:** $F(\theta) = \mathbf{w}^{\mathrm{H}}\mathbf{a}(\theta)$.

Given that the l_0 norm minimization is nonconvex and hard to solve, a common alternative is the minimization of l_1 norm

$$\min_{\Gamma} \ \|\mathbf{G}(\Gamma)\|_1 \tag{28}$$

where $\|\cdot\|_1$ denotes the l_1 norm operation.

To further enhance the sparsity of Γ, we use the reweighted l_1 minimization in [30] which can bring the weighted l_1 criterion as close as possible to the l_0 criterion. Moreover, the larger coefficients are penalized more heavily than smaller coefficients for l_1 norm. Then, we have the algorithm model by combining constraints in (10), (11), (19), and (20) as

$$\min_{\Gamma, \mathbf{r}_w} \ \sum_{r=1}^{R} \mathbf{A}^{(i)} \odot \mathbf{G}^{(i)}(\Gamma) \tag{29a}$$

$$\text{s.t. } l(\theta) \le \mathbf{r}_w^{\mathrm{T}}\mathbf{b}(\theta) \le u(\theta), \quad \theta \in \Omega_m \tag{29b}$$

$$\mathbf{r}_w^{\mathrm{T}}\mathbf{b}(\theta) \le \rho(\theta), \quad \theta \in \Omega_s \tag{29c}$$

$$\mathbf{r}_w^{\mathrm{T}}\mathbf{b}(\theta) \le \rho(\theta) + \gamma(\theta), \quad \theta \in \Omega_{r,1} \cup \Omega_{r,2} \tag{29d}$$

$$\mathbf{r}_w^{\mathrm{T}}\mathbf{b}(\theta) \ge 0 \tag{29e}$$

$$r_w(-n) = r_w^*(n), \quad n = 1, \ldots, N-1 \tag{29f}$$

$$r_w(0) \ge 0 \tag{29g}$$

$$\gamma(\theta) \ge 0 \tag{29h}$$

with $\mathbf{A}^{(i)} = [\alpha_1^{(i)}, \alpha_2^{(i)}, \ldots, \alpha_R^{(i)}]^{\mathrm{T}}$, and $\alpha_r^{(i)} = (|(1/r)(g^{(i-1)}(\gamma_1) + g^{(i-1)}(\gamma_2) + \cdots + g^{(i-1)}(\gamma_r))| + \epsilon)^{-1}$, where ϵ denotes a positive parameter and i stands for the ith iteration. $\odot$ denotes the Hadamard product. Compared to the iterative optimization process, the complexity of recovering $\mathbf{w}$ can be ignored. Using the specific interior-point method, namely the primal-dual path-following method [31] (i.e., the SDPT3 CVX solver), the worst-case complexity of proposed RD-SF method in a single iteration is $\mathcal{O}(\max\{P, 2N-1\}^2 N^{(1/2)} \log(1/\eta))$. P is the number of constraints and $\eta > 0$ denotes the solution accuracy. Algorithm flow of RD-SF is summarized in Algorithm 1.

C. Broadband Beampattern Synthesis via Two-Step SRV

For broadband beampattern synthesis, steering vectors $\mathbf{a}(f_k, \theta)$ are different at different frequency bins

$$\mathbf{a}(f_k, \theta) = \left[1, e^{j2\pi f_k d \sin(\theta)/c}, \ldots, e^{j2\pi f_k (N-1) d \sin(\theta)/c}\right]^{\mathrm{T}} \tag{30}$$

with $k = 1, 2, \ldots, K$. Naturally, vector in (6) is also be rewritten

$$\mathbf{b}(f_k, \theta) = \left[e^{-j2\pi f_k (N-1) d \sin(\theta)/c}, \ldots, 1, \ldots, e^{j2\pi f_k (N-1) d \sin(\theta)/c}\right]^{\mathrm{T}}. \tag{31}$$

Thus, our purpose is to obtain $\mathbf{r}_w(f_k)$ and $\mathbf{w}(f_k)$.

According to the SRV-class methods [18], [23] and the two-step method [26], we utilize a two-step SRV strategy to synthesize FI broadband beampattern. By combining the synthesis strategy of two-step method and the constraints of SRV, our proposed RD-SF-B method can avoid the mainlobe distortion that may occur in the two-step method, while reducing redundant SRV constraints.

Algorithm 2 Proposed RD-SF-B Algorithm

1: Set working frequency band $[f_L, f_U]$ and divide it into $f_k, k = 1, 2, \ldots, K$.
2: Select $f_0 = f_L$ as the reference frequency.
3: Do **Algorithm 1** and obtain the beampattern at reference frequency f_0.
4: Obtain $F(f_0, \theta), \Omega_{\min}, \Omega_{\text{side}}$.
5: **Input:** $u(\theta), l(\theta), \rho(\theta), \Omega_m, \Omega_{\min}, \Omega_{\text{side}}$.
6: **for** $k = 1 \rightarrow K$ **do**
7: Solve problem (32) and obtain desired $\mathbf{r}_w(f_k)$.
8: Get $\mathbf{w}(f_k)$ through the SF method.
9: **end for**
10: **Output:** $F(f_k, \theta) = \mathbf{w}^{\mathrm{H}}(f_k)\mathbf{a}(f_k, \theta)$.

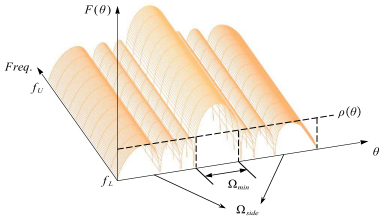

Fig. 2. Illustration for the broadband FI beam.

Within our concerned frequency bins $[f_L, f_H]$, it is known that the higher the frequency, the narrower the mainlobe. Naturally, let the lowest frequency f_L be the reference one f_0, broadening mainlobe of other frequencies can lead to a constant beamwidth. After the first step of solving (29) at f_0, we obtain the $\mathbf{r}_w(f_0)$ and the minimum mainlobe angular region $\Omega_{\min}$ and the rest of angles are sidelobe region Ω_{side}, both regions are shown in Fig. 2. The second step is to apply SRV constraints on the mainlobes at other frequencies. With this scheme, the optimization model of the second step is

$$\min_{\mathbf{r}_w(f_k)} \quad \tau \tag{32a}$$

$$\text{s.t. } l(\theta) \le \mathbf{r}_w^{\mathrm{T}}(f_k)\,\mathbf{b}(f_k, \theta) \le u(\theta), \quad \theta \in \Omega_m \tag{32b}$$

$$\mathbf{r}_w^{\mathrm{T}}(f_k)\,\mathbf{b}(f_k, \theta) \le \rho(\theta), \quad \theta \in \Omega_{\text{side}} \tag{32c}$$

$$\left|\mathbf{r}_w^{\mathrm{T}}(f_k)\,\mathbf{b}(f_k, \theta) - \mathbf{r}_w^{\mathrm{T}}(f_0)\,\mathbf{b}(f_0, \theta)\right| \le \tau, \quad \theta \in \Omega_{\min} \tag{32d}$$

$$\mathbf{r}_w^{\mathrm{T}}(f_k)\,\mathbf{b}(f_k, \theta) \ge 0 \tag{32e}$$

$$r_w(f_k, -n) = r_w^*(f_k, n), \quad n = 1, \ldots, N-1 \tag{32f}$$

$$r_w(f_k, 0) \ge 0 \tag{32g}$$

where τ is the error of the SRV constraints on mainlobe. And it is worth mentioning that the SRV-class methods need rely on experience to set the error. However, due to its two-step synthesis scheme, RD-SF-B method can automatically obtain this error as the objective function for optimizing the second-step. Meanwhile, this scheme can also ensure the consistency of the mainlobe as much as possible. Algorithm flow of RD-SF-B is given in Algorithm 2.

IV. Simulations

In this section, we will demonstrate the performance of our proposed method. Taking a ULA with $N = 20$ elements with spacing of $d = \lambda/2$ into consideration, simulation results are given to show the feasibility of RD-SF and RD-SF-B algorithms.

A. Focused Beampattern With Different Iterations

For clearly demonstrating the convergence process of the proposed algorithm, in this section, we use our proposed algorithm to synthesize a focused beampattern with mainlobe pointing at 20° and

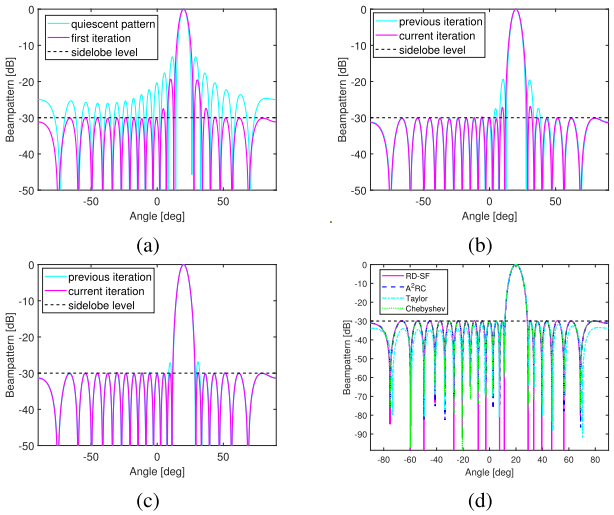

Fig. 3. Focused beampattern. (a) Beampatterns at the first iteration. (b) Second iteration. (c) Third iteration. (d) Beampatterns by different methods.

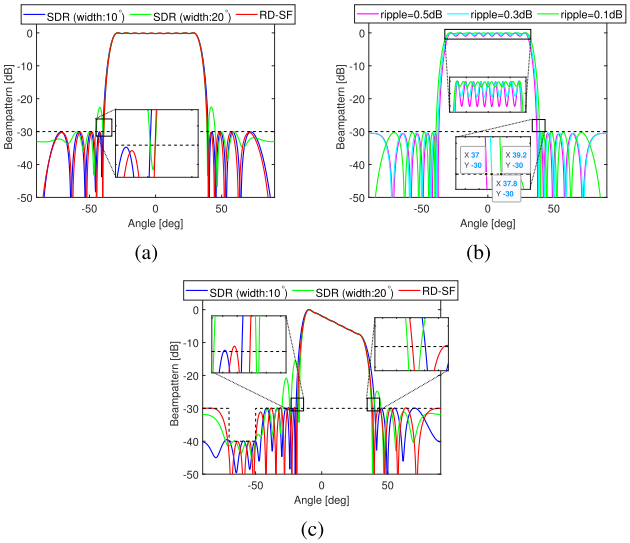

Fig. 4. Flat-top beampattern. (a) Flat-top beampattern using different methods. (b) Flat-top beampattern with different ripple level. (c) Shaped beampattern with nonuniform mainlobe and sidelobe level.

sidelobe upper level of −30 dB. The initial relaxation region is set as $[0°, 40°]$. Beampatterns at different iterations are shown in Fig. 3.

As the number of iterations increases, the synthesized pattern gradually approaches the ideal pattern and stabilizes after the third iteration, highlighting the convergence performance of our proposed algorithm. In addition, we also compare with Chebyshev method, Taylor method, and A^{2}RC [32] method whose simulation results are given in Fig. 3(d). In this situation, performance of these methods are almost identical. This also proves that the proposed method can successfully achieve the synthesis of the minimum mainlobe width.

B. Shaped Beampattern Synthesis

In this section, we simulate the shaped beampatterns separately under uniform and nonuniform mainlobe and sidelobe levels. As a comparison, we simulated the SDR method [10] under two different widths of relaxation intervals, and also simulated the proposed algorithm under a wider relaxation region.

1) Flat-Top Beampattern With Uniform Sidelobe Level: The flat-top width is set as 60° ($[-30°, 30°]$) with ripple level of 0.1 dB.

TABLE I

MAINLOBE WIDTH AND RUNNING TIME FOR DIFFERENT METHODS

	Uni.Shape		Non-Uni.Shape	
Methods	Width	Time	Width	Time
SDR (width:10°)	79.56°	159.96 s	59.48°	210.95 s
SDR (width:20°)	94.96°	110.92 s	74.93°	135.72 s
RD-SF	78.36°	63.23 s	56.66°	68.70 s

TABLE II

MAINLOBE WIDTH AND RUNNING TIME FOR DIFFERENT METHODS

Methods	Width	Time
Two-Step Method	13.72°	516.86 s
l_∞-SRV Method	13.66°	1616.47 s
RD-SF-B Method	13.72°	514.38 s

For comparison, SDR method with transition region widths of 10° and 20° are considered. Simulation results are shown in Fig. 4(a), and mainlobe width and running time are given in Table I (Uni.Shape).

It is easily to find that under this simulation condition, the transition region width of 10° is more suitable for the SDR method than 20°. This further indicates the SDR method requires proper setting of the mainlobe width to obtain the ideal pattern. Setting the mainlobe width too wide can result in a synthesized beampattern that does not meet the requirements. On the contrary, the RD-SF method can still converge to the minimum mainlobe width and obtain an ideal pattern even when the initial width is set too wide. Additionally, our proposed algorithm also has significant advantage in running time.

Based on our proposed algorithm, with the same initial setting in Fig. 4(a), the simulation results at different mainlobe ripple levels is shown in Fig. 4(b). It can be seen that as the mainlobe ripple level decreases, the mainlobe width of the synthesized patterns in our proposed algorithm gradually increases, which conforms to the trade-off relationship of mainlobe width and ripple level.

2) Shaped Beampattern With Nonuniform Mainlobe and Sidelobe Level: To demonstrate the universality of our proposed algorithm, this simulation gradually decreases the mainlobe level in $[-10°, 30°]$ (width of 40°), and adds a -40 dB sidelobe notch between $[-70°, -50°]$. Simulation results are shown in Fig. 4(c), and the mainlobe width and running time are given in Table I (Nonuni.Shape).

Results confirm that the mainlobe and sidelobe synthesized by both the SDR and proposed methods meet the specified requirements. Similarly, for the SDR method, it is still necessary to set an appropriate mainlobe width. For our proposed method, beampattern with the narrowest mainlobe width under relatively complex conditions can be synthesized automatically, and its running time is still much faster.

C. Broadband Beampattern Synthesis

In this section, we concentrate on synthesizing FI broadband beampattern. Since the two-step SRV scheme of RD-SF-B method combines the advantages of two-step method and SRV-class methods, these two methods will be used as comparisons.

1) Focused Broadband Beampattern Comparison: Here, we will separately simulate the l_∞-SRV method [23], the two-step method [26], and our proposed method in the case of synthesizing focused FI broadband beampattern. Frequency band is set to [f_L = 1.4 GHz, f_U = 2.4 GHz] and is discretized to 21 uniform frequency bins. With mainlobe at 0° and upper sidelobe level at -25 dB, we set the reference frequency as $f_0 = f_L$ and initial mainlobe width is set as $[-20°, 20°]$. Simulation results obtained by these three methods are shown in Fig. 5, and mainlobe width and running time are also given in Table II.

All three methods synthesize broadband beampatterns with nearly consistent mainlobe widths (≈13.7°). However, the two-step method exhibits mainlobe distortion with increasing bandwidth,

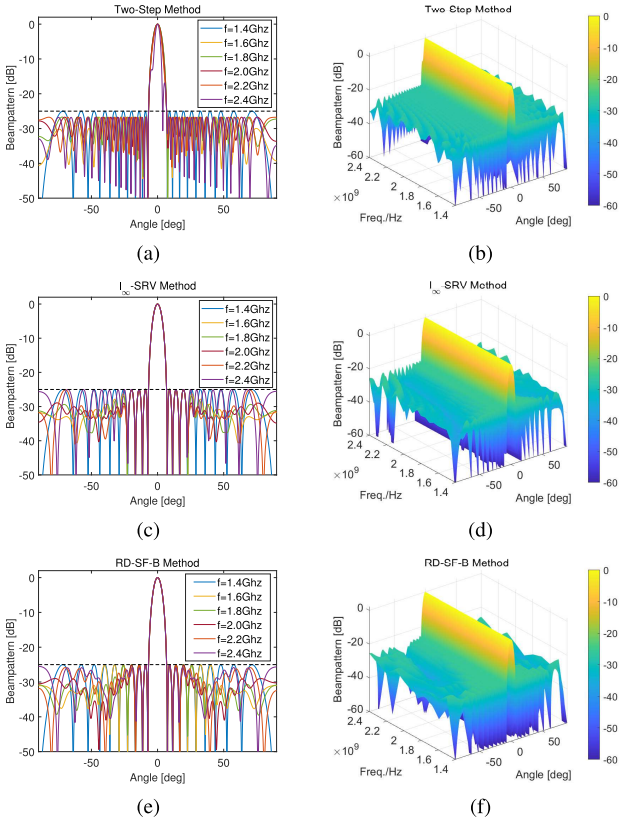

Fig. 5. Focused FI broadband beampatterns. (a) Beampatterns at discrete frequencies of two-step method. (b) 3-D FI beampattern of two-step method. (c) Beampatterns at discrete frequencies of l_∞-SRV method. (d) 3-D FI beampattern of l_∞-SRV method. (e) Beampatterns at discrete frequencies of RD-SF-B. (f) 3-D FI beampattern of RD-SF-B.

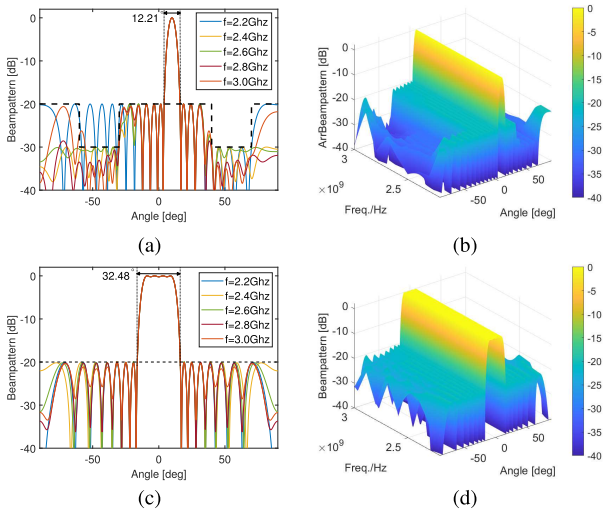

Fig. 6. Shaped FI broadband beampattern. (a) Beampatterns with nonuniform sidelobe at discrete frequencies of RD-SF-B. (b) 3-D FI beampattern with nonuniform sidelobe of RD-SF-B. (c) Beampatterns with flat-top at discrete frequencies of RD-SF-B. (d) 3-D FI beampattern with flat-top of RD-SF-B.

as demonstrated in Fig. 5(a). The l_∞-SRV method suffers from either empirically set or relaxation-region-matched SRV constraints; excessively broad constraint ranges incur significant computational overhead (Table II). Our RD-SF-B method synthesizes the advantages of both approaches while circumventing these limitations, achieving desired beampattern with enhanced stability and efficiency.

2) Shaped Broadband Beampattern: To further demonstrate the effectiveness of RD-SF-B method in synthesizing shaped pattern, we steer the mainlobe to 10° and add two notches with upper limit level of −30 dB. One is at frequency range of [2.4, 2.8 GHz], the other is at frequency range of [2.2, 3.0 GHz]. In addition, we also consider the flat-top FI beam, setting 0.1 dB ripple level at $[-10°, 10°]$, −20 dB upper sidelobe level, and initial mainlobe region as $[-30°, 30°]$. Simulation results of these two conditions are both shown in Fig. 6.

FI broadband beampatterns were synthesized in 211.50 and 124.46 s for two different conditions, respectively. These results demonstrate our method's capability to precisely control beampatterns within specified angular and frequency ranges.

V. Conclusion

This communication presents the RD-SF algorithm for beampattern synthesis with auto-determined minimum mainlobe width and its broadband extension RD-SF-B for FI broadband patterns. The auto-determination capability eliminates potential disadvantages caused by manual mainlobe specification. The RD-SF method efficiently solves nonconvex optimization problems while significantly improving computational efficiency. Furthermore, RD-SF-B prevents mainlobe distortion by eliminating redundant constraints without requiring empirical error settings. Current implementations focus on ULA due to SF requirements, with extension to arbitrary array geometries constituting ongoing research.

References

[1] R. J. Mailloux, *Phased Array Antenna Handbook*. Norwood, MA, USA: Artech House, 2017.

[2] C. L. Dolph, "A current distribution for broadside arrays which optimizes the relationship between beam width and side-lobe level," *Proc. IRE*, vol. 34, no. 6, pp. 335–348, Jun. 1946.

[3] H. Unz, "Linear arrays with arbitrarily distributed elements," *IRE Trans. Antennas Propag.*, vol. 8, no. 2, pp. 222–223, Mar. 1960.

[4] K.-K. Yan and Y. Lu, "Sidelobe reduction in array-pattern synthesis using genetic algorithm," *IEEE Trans. Antennas Propag.*, vol. 45, no. 7, pp. 1117–1122, Jul. 1997.

[5] D. G. Kurup, M. Himdi, and A. Rydberg, "Synthesis of uniform amplitude unequally spaced antenna arrays using the differential evolution algorithm," *IEEE Trans. Antennas Propag.*, vol. 51, no. 9, pp. 2210–2217, Sep. 2003.

[6] D. W. Boeringer and D. H. Werner, "Particle swarm optimization versus genetic algorithms for phased array synthesis," *IEEE Trans. Antennas Propag.*, vol. 52, no. 3, pp. 771–779, Mar. 2004.

[7] B. Stephen and L. Vandengerghe, *Convex Optimization*. Cambridge, U.K.: Cambridge Univ. Press, 2004.

[8] H. Lebret and S. Boyd, "Antenna array pattern synthesis via convex optimization," *IEEE Trans. Signal Process.*, vol. 45, no. 3, pp. 526–532, Mar. 1997.

[9] Z.-Q. Luo, W.-K. Ma, A. M. So, Y. Ye, and S. Zhang, "Semidefinite relaxation of quadratic optimization problems," *IEEE Signal Process. Mag.*, vol. 27, no. 3, pp. 20–34, May 2010.

[10] B. Fuchs, "Application of convex relaxation to array synthesis problems," *IEEE Trans. Antennas Propag.*, vol. 62, no. 2, pp. 634–640, Feb. 2014.

[11] B. Fuchs, "Shaped beam synthesis of arbitrary arrays via linear programming," *IEEE Antennas Wireless Propag. Lett.*, vol. 9, pp. 481–484, 2010.

[12] B. Fuchs, A. Skrivervik, and J. R. Mosig, "Shaped beam synthesis of arrays via sequential convex optimizations," *IEEE Antennas Wireless Propag. Lett.*, vol. 12, pp. 1049–1052, 2013.

[13] Q. Shen, W. Liu, W. Cui, S. Wu, Y. D. Zhang, and M. G. Amin, "Low-complexity direction-of-arrival estimation based on wideband co-prime arrays," *IEEE/ACM Trans. Audio, Speech, Language Process.*, vol. 23, no. 9, pp. 1445–1456, Sep. 2015.

[14] D. B. Ward, R. A. Kennedy, and R. C. Williamson, "FIR filter design for frequency invariant beamformers," *IEEE Signal Process. Lett.*, vol. 3, no. 3, pp. 69–71, Mar. 1996.

[15] W. Liu and S. Weiss, "Design of frequency invariant beamformers for broadband arrays," *IEEE Trans. Signal Process.*, vol. 56, no. 2, pp. 855–860, Feb. 2008.

[16] M. Crocco and A. Trucco, "Design of robust superdirective arrays with a tunable tradeoff between directivity and frequency-invariance," *IEEE Trans. Signal Process.*, vol. 59, no. 5, pp. 2169–2181, May 2011.

[17] C. Zhu, X. Li, Y. Liu, L. Liu, and Q. H. Liu, "An extended generalized matrix pencil method to synthesize multiple-pattern frequency-invariant linear arrays," *IEEE Antennas Wireless Propag. Lett.*, vol. 16, pp. 2311–2315, 2017.

[18] H. Duan, B. P. Ng, C. M. S. See, and J. Fang, "Applications of the SRV constraint in broadband pattern synthesis," *Signal Process.*, vol. 88, no. 4, pp. 1035–1045, Apr. 2008.

[19] Z. Teng et al., "Phased-array beampattern synthesis with a tradeoff between sparsity and sidelobe level," *Signal Process.*, vol. 214, Jan. 2024, Art. no. 109227.

[20] D. Shiung, "A trick for designing composite filters with sharp transition bands and highly suppressed stopbands [tips & tricks]," *IEEE Signal Process. Mag.*, vol. 39, no. 5, pp. 70–76, Sep. 2022.

[21] K. Tang and X. Zhang, "Auto-determining mainlobe width for beampattern synthesis via relaxation optimization," *IEEE Signal Process. Lett.*, vol. 29, pp. 314–318, 2022.

[22] W. Peng, T. Gu, Y. Zhuang, Z. He, and C. Han, "Pattern synthesis with minimum mainlobe width via sparse optimization," *Digit. Signal Process.*, vol. 128, Aug. 2022, Art. no. 103632.

[23] Z. Teng, L. Gao, L. Gan, H. Liao, K. Du, and H. Jiang, "Accurate spatial-frequency response controllable frequency invariant beampattern synthesis with minimum beamwidth," *IEEE Trans. Antennas Propag.*, vol. 71, no. 7, pp. 6266–6271, Jul. 2023.

[24] A. Zhang, S. Lei, W. Yang, J. Tian, H. Hu, and L. Xiao, "Mainlobe/sidelobe region gap minimization for shaped-beam pattern synthesis via antenna array," *IEEE Antennas Wireless Propag. Lett.*, vol. 23, pp. 144–148, 2024.

[25] M. Huan, J. Liang, Y. Ma, W. Liu, Y. Wu, and Y. Zeng, "Optimization of high-resolution and ambiguity-free sparse planar array geometry for automotive MIMO radar," *IEEE Trans. Signal Process.*, vol. 72, pp. 4332–4348, 2024.

[26] W. Peng, T. Gu, X. Zhang, Z. He, and C. Han, "Broadband pattern synthesis with minimum mainlobe beamwidth and sidelobe level control," *IGARSS*, vol. 56, pp. 2983–2986, Mar. 2022.

[27] Z. Teng, H. Zhang, J. An, L. Gan, H. Li, and C. Yuen, "Low-complexity frequency invariant beamformer design based on SRV-constrained array response control," in *Proc. IEEE 99th Veh. Technol. Conf. (VTC-Spring)*, Jun. 2024, pp. 1–5.

[28] S.-P. Wu, S. Boyd, and L. Vandenberghe, "FIR filter design via semidefinite programming and spectral factorization," in *Proc. 35th IEEE Conf. Decis. Control*, vol. 1, Dec. 1996, pp. 271–276.

[29] Z. L. Yu, M. H. Er, and W. Ser, "A novel adaptive beamformer based on semidefinite programming (SDP) with magnitude response constraints," *IEEE Trans. Antennas Propag.*, vol. 56, no. 5, pp. 1297–1307, May 2008.

[30] B. Fuchs, "Synthesis of sparse arrays with focused or shaped beampattern via sequential convex optimizations," *IEEE Trans. Antennas Propag.*, vol. 60, no. 7, pp. 3499–3503, Jul. 2012.

[31] C. Helmberg, F. Rendl, R. J. Vanderbei, and H. Wolkowicz, "An interior-point method for semidefinite programming," *SIAM J. Optim.*, vol. 6, no. 2, pp. 342–361, 1996.

[32] X. Zhang, Z. He, B. Liao, X. Zhang, Z. Cheng, and Y. Lu, "A^{2}RC: An accurate array response control algorithm for pattern synthesis," *IEEE Trans. Signal Process.*, vol. 65, no. 7, pp. 1810–1824, Jul. 2017.